Lachmar *et al. Geothermal Energy* (2023) 11:21
https://doi.org/10.1186/s40517-023-00264-4

Geothermal Energy

RESEARCH Open Access

Validation of Play Fairway Analysis of the geothermal potential of Camas Prairie, south-central Idaho, by an exploration well

Thomas E. Lachmar[1*], Ghanashyam Neupane[2], Sabodh K. Garg[3], Patrick F. Dobson[4], Connor J. Smith[1], Dennis L. Newell[1], John W. Shervais[1], James P. Evans[1] and Leland L. Mink[5]

*Correspondence: tom.lachmar@gmail.com

[1] Department of Geosciences, Utah State University, Logan, UT 84322-4505, USA
[2] Idaho National Laboratory, Idaho Falls, ID 83402, USA
[3] Geologica Geothermal Group Inc., San Diego, CA 94103, USA
[4] Lawrence Berkeley National Laboratory, Berkeley, CA 94720, USA
[5] Mink GeoHydro Inc., Worley, ID 83876, USA

Abstract

Play Fairway Analysis (PFA) methodology was adapted for geothermal exploration at Camas Prairie, Idaho. Geophysical data, structural and geologic mapping, volcanic rock ages and vent locations, and the distribution of thermal springs and wells all indicated a relatively high geothermal potential along the southern margin of the Prairie. An exploration well (USU Camas-1) was drilled to a depth of 618.3 m to validate the PFA. A permeable zone was encountered at ~ 357.5 m with a maximum measured temperature of ~ 80 °C, which was suppressed following the injection of cold water. A moderate transmissivity of ~ 0.25–1 cm^2/s estimated from an injection test as well a seasonal artesian flow at ~ 0.7 L/s corroborate the presence of a permeable zone. The existence of a lacustrine clay seal was confirmed near the bottom of the basin-fill sediment occupying the upper 314 m of the well. Geothermometers suggest the USU Camas-1 well water equilibrated at a reservoir temperature of ~ 120 °C. Based on the locations of both thermal and cold wells, geothermal fluids appear to be flowing upward along one or both of two fault systems. The presence of young basalts and elevated helium isotope ratios suggest that the heat source of Camas Prairie is magmatic. However, the faults may be acting as a conduit for geothermal fluids to rise from great depth without a shallow magmatic source being present. Camas Prairie is a promising area for geothermal development, but the relatively low reservoir temperatures indicate this resource may not be suitable for electric generation. Perhaps the best use would be for heating.

Keywords: Geophysical logs, Temperature logs, Injection test, Geochemistry, Geothermometers

Introduction

The Snake River Plain (SRP) volcanic province, southern Idaho, has long been considered a target for geothermal development. It overlies a thermal anomaly extending deep into the mantle and is one of the highest heat flow provinces in North America (Blackwell 1989; Blackwell and Richards 2004). Idaho was ranked third among western states for potential geothermal power production, with 855 MW of near-term economic potential resources (Western Governors' Association 2006). However, a

regional characterization of geothermal resource potential has not been performed previously, as systematic exploration has been hindered by the presence of an overlying cold groundwater system (Lachmar et al. 2017) and the lack of conceptual models for the geothermal systems in the region.

Play Fairway Analysis (PFA) is an approach to exploration pioneered by the petroleum industry that integrates data at the regional or basin scale to define exploration targets (plays). These data are evaluated systematically to define areas that have a high likelihood of success. PFA provides greater technical rigor than traditional exploration approaches, and facilitates decision-making even when data are sparse or incomplete (Shell Exploration and Production 2013).

Camas Prairie, south-central Idaho, is a representative geothermal play for the central SRP (Fig. 1). It has elevated heat flow (Blackwell 1989), and Quaternary volcanism in the southern part of the basin suggests a magmatic heat source (Clemens and Wood 1993; Gaschnig et al. 2011; Honjo 1990; Shervais et al. 2002). It was identified using PFA as a region with relatively high geothermal potential (Glen et al. 2017; Shervais et al. 2018), and was selected for validation by drilling an exploration well (Shervais et al. 2020).

The well site selected lies 600 to 800 m above the projected intersection of two fault systems, and was expected to be a productive hydrothermal zone and a good location to drill (Glen et al. 2017). The exploratory USU Camas-1 well was first drilled to a depth of 491.3 m below ground surface (bgs) via rotary methods in the fall of 2018. Then, after a 10-month hiatus, the well was extended by coring to a total depth (TD) of 618.3 m bgs. The following data were collected from USU Camas-1 to assess the geothermal potential of Camas Prairie: the lithology and mineralogy of cuttings and core, geophysical data, temperature data, the results of an injection test, and water chemistry, specifically major cations and anions as well as stable isotopes of oxygen and hydrogen.

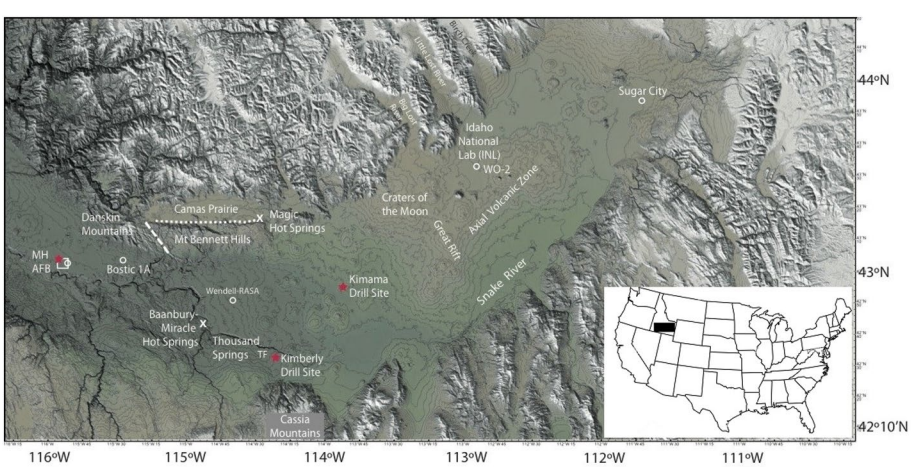

Fig. 1 Shaded relief-topographic map of SRP. Derived from NASA 10 m DEM data and contoured at 30 m intervals in GeoMap App. Lowest elevations are green, and highest are white. Major features discussed in text are labeled. Project Hotspot drill sites = red stars; other drill sites = white circles. Hot springs shown with small x. Mount Bennett Hills range-front fault zone indicated with white dotted line; boundary between NE-dipping Danskin Mountains and S-dipping Mount Bennett Hills indicated with white dashed line (Shervais et al. 2015)

Background

Geologic and hydrologic setting

Camas Prairie, Idaho (Fig. 1), lies north of the SRP volcanic province (SRP-VP) and formed largely coincident with SRP volcanism in the late Pliocene and Pleistocene. The SRP-VP formed in response to interactions with the Yellowstone–SRP hotspot (mantle plume) during ESE-trending movement of the North American plate in the late Neogene (from ~ 17 Ma; Smith and Braile 1994). The Yellowstone–SRP hotspot is thought to provide the excess heat that drives volcanism and geothermal activity (Smith et al. 2009). Basaltic volcanism has continued through the Holocene.

Camas Prairie is a ~ 70 × 16 km east–west, structural half-graben bounded by a range-front normal fault along the northern base of the Mount Bennett Hills to the south, and by a gentle down warp in the Idaho batholith on the north (Cluer and Cluer 1986; Garwood et al. 2014). The Idaho batholith bounds the northern margin of Camas Prairie. It is composed of late Cretaceous (67–83 Ma) biotite granodiorite and granite (Kiilsgaard and Lewis 1985; Gaschnig et al. 2011). Eocene (44–51 Ma) dacites and andesites overlie the Idaho batholith and crop out in the Mount Bennett Hills south of Camas Prairie (Clemens and Wood 1993; Gaschnig et al. 2011). The Mount Bennett Hills consist of Miocene (9–10 Ma) rhyolites overlain by younger basalt flows. The rhyolites originated from eruptive centers in the SRP (Honjo 1990; Clemens and Wood 1993).

Camas Prairie is bounded on the east by the Magic Reservoir Known Geothermal Area, which is associated with Pliocene rhyolites (Honjo 1990; Clemens and Wood 1993) that obstructed the outlet of the Camas Prairie basin in the Magic Reservoir area. During the Pliocene, poorly sorted lacustrine sediments along with valley fill and alluvium were deposited, filling the basin into the Pleistocene. The deposits range from coarse-grained at the base of the Idaho batholith to the north to fine-grained near the center of the basin, with a depocenter near the southern margin of the basin close to the uplifted Mount Bennett Hills. Sediment is derived largely from the Idaho batholith.

The Mount Bennett Hills are highly faulted and a few of these faults can be mapped into the basin center (Shervais et al. 2016). Most prominent is a WNW-trending through-going fault system named for a distinct volcanic crater ("The Pothole"). The Pothole fault system divides the Mount Bennett Hills into eastern and western blocks, with NW-trending faults dominating the eastern block and NE-trending faults dominating the western block (Shervais et al. 2017). Offset of "The Pothole" constrains the minimum age of local faulting to less than 700 ka.

Shallow aquifers beneath Camas Prairie are in lacustrine and basin-fill sediments, and are both unconfined and confined. Hydraulic heads in the geothermal fluids at depth are, at times, great enough to produce flow at the surface from wells. Interbedded clayey sand and sandy clay act as confining layers for these pressurized fluids (Smith 2022).

Play Fairway Analysis

PFA of Camas Prairie was carried out as part of a broader study of the SRP volcanic province (Nielson and Shervais 2014; Shervais et al. 2016; DeAngelo et al. 2021a, 2021b). The approach, described in detail by Shervais et al. (in press) and DeAngelo et al. (in press), consisted of three phases. Phase 1 compiled published data into an ArcGIS-based

database. Phase 2 collected additional geophysical, geochemical, and geologic data, as needed, to fill data gaps identified in Phase 1. Phase 3 selected a single prospect to validate the efficacy of the predictions by drilling an exploration well.

The ArcGIS database into which the data obtained during Phases 1 and 2 were compiled contained multiple data layers. These data layers were processed using either density functions (simple or kernel density) or interpolations (radial basis function, inverse distance weighted, or empirical Bayesian Kriging) to produce evidence layers (Shervais et al. 2016; DeAngelo et al. 2021a, 2021b). Risk maps represent the product of evidence and confidence layers, and are the basic building blocks used to construct Common Risk Segment (CRS) maps for the three critical geothermal resource parameters: heat, permeability, and seal. These three maps then were combined into a Composite Common Risk Segment (CCRS) map (Shervais et al. 2017).

Based on the Phase 1 results, the Camas Prairie region was chosen for further study in Phase 2 to fill data gaps and refine assessment tools. New field data collected in Phase 2 included geologic and structural mapping and sampling, geophysical studies, and water chemistry. Structural mapping of faults and fault intersections revealed that the most important fault system is the Pothole fault. Twelve samples were collected from young volcanic vents for $^{40}Ar/^{39}Ar$ age dating by the Geochronology Laboratory at Oregon State University (Shervais et al. 2017). The Pothole fault offsets The Pothole volcanic crater that was dated at 692 ka (Shervais et al. 2018).

Geophysical studies included active source reflection seismic, gravity, and magnetic surveys, and a magnetotelluric (MT) field campaign (Glen et al. 2017). Gravity and magnetic maps identified the Pothole fault and a range-front fault system that trends approximately east–west along the northern edge of the Mount Bennett Hills. The intersection of these two fault systems may control the location of the hot springs. MT data documented a low-resistivity structure interpreted to represent a clay cap (Glen et al. 2017).

Natural springs and wells were sampled, and several previously sampled locations were re-sampled to assess seasonal variations. The samples were analyzed for major and trace elements, and stable isotopes of oxygen, hydrogen, and helium. The analytical results indicated that the hydrothermal waters are dominantly meteoric in origin, with some modification from water–rock interaction at elevated temperatures. Calculations using cation, silica, and multicomponent geothermometers for samples from the southern margin of Camas Prairie yielded equilibrium reservoir temperature estimates of ~ 110 °C (Neupane et al. 2014, 2017).

The CCRS map for Camas Prairie (Fig. 2) shows that the most favorable area is at the southern end of the Pothole fault system, which trends northwest–southeast across the map. The resource is indicated by thermal springs that cluster along the fault and elevated helium isotope ratios (Dobson et al. 2015). Target depths were estimated to be as shallow as 500–700 m.

Methods

Field methods

The US Geological Survey (USGS) Research Drilling unit drilled the USU Camas-1 exploration well in three stages. Stage 1 drilling commenced in September 2018 using a top head TH60DH rig to drill via mud rotary to 347.5 m bgs. Stage 2 drilling commenced

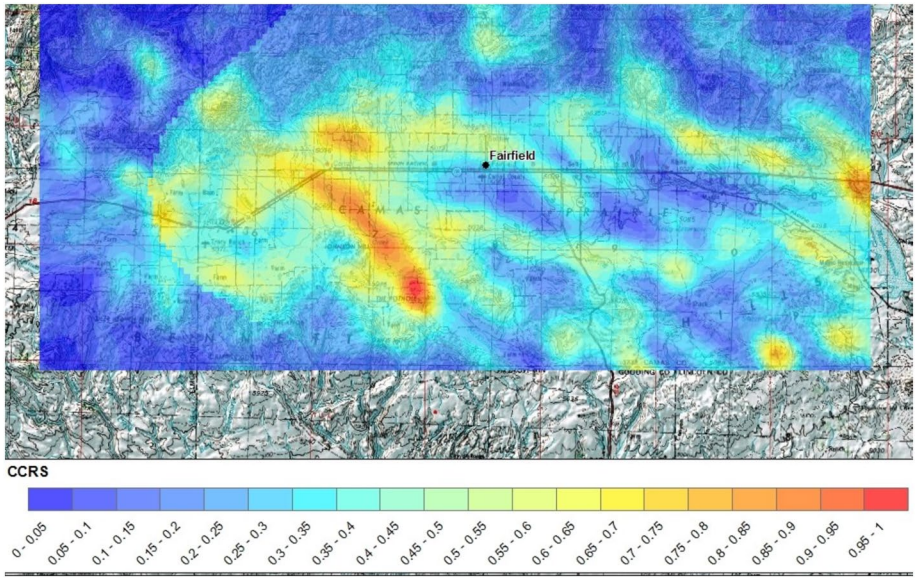

Fig. 2 CCRS map of Camas Prairie (Shervais et al. 2017). Scale represents favorability scores ranging from zero (lowest, blue) to one (highest, red). The most favorable areas are along the Pothole fault system, trending NW–SE

in October 2018, when the well was deepened to 491.3 m bgs. Finally, for Stage 3, the well was cored to TD at 618.3 m bgs in the fall of 2019 using a Christensen CS 1000 P6L rig. Drilling details can be found in Smith (2022).

The lithology of cuttings and core was determined by in-field inspection, as well as post-drilling petrographic examination of thin sections and laboratory analysis. Mineralogy was determined in the field directly by examining the cuttings and core under hand lenses, applying dilute HCl to the samples, and examining them under a binocular microscope.

Geophysical logs were collected by the USGS Research Drilling Geophysical unit with a wireline sonde after each stage prior to setting casing or after removal of drill rods. The wireline logs included caliper, natural gamma, resistivity, conductivity, spontaneous potential (SP), and delta T. In addition, a downhole temperature log was obtained using an HOBO® device produced by Onset Computer Corporation. In October 2018, after the well was deepened to 491.3 m bgs, a reservoir test was carried out by the USGS Geophysical unit under the supervision of Colin Goranson by sealing the well and injecting fluids.

The discharge rate was measured using the bucket and stopwatch method in July 2019 when the well was flowing artesian, while it was still 491.3 m deep. Water samples also were collected under artesian conditions in August 2019 using standard groundwater sampling techniques (USGS 2006). Prior to sampling, the well was opened and purged for over 2 h. Temperature, pH, and electrical conductivity were measured in the field using a portable meter. Alkalinity of the water was determined with end-point titration using Hach's digital titrator.

To collect water samples, silicone tubing was placed inside the well flow port. This hose was attached to coiled stainless steel tubing surrounded by ice to lower the temperature of the scalding samples. Water samples for cations were field filtered into acid-cleaned

500 mL HDPE bottles using 0.45 μm filters, and acidified using concentrated Optima® grade nitric acid to pH < 2. Samples for anions were collected into 250 mL HDPE bottles. Water samples for stable isotope determination of $\delta^{18}O$ and $\delta^{2}H$ were collected in amber glass vials with no headspace. Prior to collection, each sample bottle/vial was rinsed three times with the sample water. Water samples then were transported directly to the laboratory for analysis.

Laboratory methods

Mineralogy of the rocks sampled by the core was determined by X-ray diffractometry (XRD) using the PANalytical X'Pert PRO XRD spectrometer at USU Geosciences X-ray Diffraction Laboratory. Mineralized surfaces of the core and alteration facies were preferentially selected for XRD analysis. X'Pert HighScore software program version 4.5 and the ICDD PDF-4 + inorganic database of reference patterns was used to match peaks automatically, while the rest of the peaks were matched manually. Potential mineral phases were refined further by petrographic analysis (Smith 2022). A clay-specific XRD analysis was not performed, but for some samples where clay was abundant, the clay mineral phases were identified by matching reference patterns.

Major- and trace-element concentrations in water samples were determined at the Utah Water Research Laboratory using a Dionex™ Ion Chromatograph (anions) and an Agilent Inductively Coupled Plasma Mass Spectrometer (cations). The $\delta^{18}O$ and $\delta^{2}H$ values were determined at the USU Department of Geosciences Stable Isotope Laboratory via continuous flow Isotope Ratio Mass Spectrometry (CF-IRMS) methods using a Thermo Scientific Delta V Advantage IRMS with Thermo Scientific high-temperature conversion elemental analysis (TC/EA) and GasBench II interfaces. Analytical uncertainty for $\delta^{18}O$ and $\delta^{2}H$ values was ± 0.1 ‰ and ± 2.0 ‰, respectively (Gehre et al. 2004).

Geothermometry

Reservoir temperatures were calculated using seven classic geothermometers. The geothermometry equations used to calculate reservoir temperature in this study are those for quartz and chalcedony (Fournier 1977), two Na/K equations (Fournier 1979; Giggenbach 1988), Na–Ca–K (Fournier and Truesdell 1973), Na–K–Ca–Mg (Fournier and Potter 1979), and K^2/Mg (Giggenbach 1988).

A multicomponent geothermometer was also applied using Reservoir Temperature Estimator (RTEst) code (Palmer et al. 2014; Neupane et al. 2015). RTEst code combines The Geochemist's Workbench (Bethke and Yeakel 2013), a geochemical modeling application, with Parameter Estimation (PEST) application (Doherty 2005, 2013) to provide a reservoir temperature estimate using composition of the thermal water and a mineral assemblage of the reservoir. For the geochemical modeling, The Geochemist's Workbench with thermo.com.V8.R6.full database derived from the thermodynamic data compiled at the Lawrence Livermore National Laboratory (Bethke and Yeakel 2013) was used.

The likely reservoir mineral assemblage was selected based on the general lithology of the reservoir and dominant fluid chemistry type. This selection method was previously developed by Palmer et al. (2014) by systematically reviewing several hydrothermal systems around the world. For the Camas Prairie geothermal reservoir, a mineral

assemblage consisting of calcite, chalcedony, K-clinoptilolite, fluorite, illite, laumontite, and K-feldspar was selected. Since the analytical results did not provide concentration of magnesium, illite was swapped for magnesium during geochemical modeling.

Results

Physical properties

The upper 314 m of the USU Camas-1 well consists of basin-fill sediment, mostly sand and pebbly sand, but a clay layer at 12–49 m bgs attests to relatively recent deposition of lacustrine sediment (Fig. 3). Clayey sand, sandy clay, and clay layers encountered from 268 to 314 m form a confining layer that inhibits fluid circulation from depth. The underlying bedrock consists of granitic rocks of the Idaho batholith, with subordinate rhyolite dikes. The granitic rocks locally are affected by hydrothermal alteration, faulting, and veins. Driller reports describe a productive zone at ~ 346.9 m. Fractures are common at this depth, and low core recovery rates suggest void space and thus permeability. Core mineralization between 344.4 and 347.5 m and the identification of hydrothermal alteration minerals, such as chlorite, gobbinsite, and clay, throughout the well below the productive zone suggest the circulation of geothermal fluids (Smith 2022).

Resistivity is low throughout the sediment section of the well, but rises in the underlying igneous basement rocks (Fig. 3). The conductivity profile displays a similar response, with some peaks and troughs opposite to those of resistivity. The SP log signature opposes resistivity throughout the entire logged (492.3 m) section of the well. The relatively low resistivity, and high conductivity and SP, near 346.9 m suggest that the rocks are permeable at this depth. Gamma ray increases near 347.5 m, reflecting the presence of rhyolite dikes due to their high potassium content. Delta T peaks to a maximum of ~ 375 μsec/ft (1230 μsec/m) at ~ 346.9 m, and then decreases to between 50 and 200 μsec/ft (165 and 655 μsec/m) near 347.5 m.

Temperature increases sharply over a 60 m interval around the productive zone at 346.9 m (Fig. 4), suggesting geothermal fluid flow. The maximum temperature recorded in the USU Camas-1 well was 80.3 °C at ~ 353.6 m, within the permeable zone that accepted cold injected water at ~ 357.5 m (Fig. 5). The temperature is nearly isothermal below the productive zone, making it difficult to calculate a geothermal gradient. The well is cased and cemented to 346.9 m, and thus, a gradient of 169 °C/km can be calculated from the surface to this depth. Since the well is isothermal below this point, the gradient is effectively 0 °C/km.

Nearby wells (Fig. 6) were logged for temperature at various times between 2010 and 2019. Wells are categorized based on their maximum temperatures. Five wells had maximum temperatures less than 30 °C. The highest temperature measured in these five wells was 29 °C in 1A. The maximum temperatures of the other four wells all were greater than 60 °C. The Barron Big Hot Spring well, the shallowest of the four, had the lowest maximum temperature of 67.2 °C.

The injection test conducted and analyzed by Garg and Goranson (2018) produced transmissivity values of ~ 0.25–1 cm^2/sec. Due to an anomaly in the rising limb of the pressure data (injection), the falling limb (recovery) was used to calculate transmissivity. The first temperature log taken 14 h after injection shows a dip in temperature centered

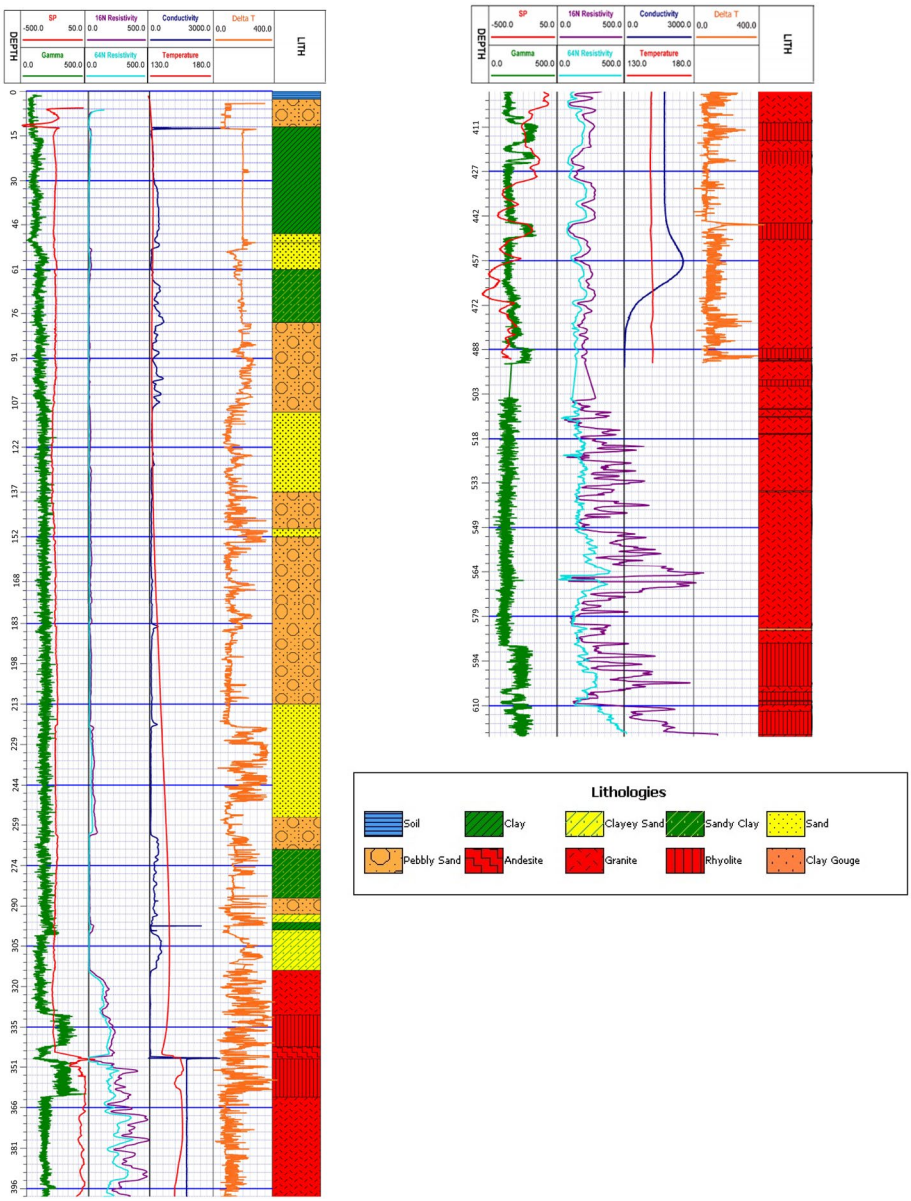

Fig. 3 Geophysical logs of SP, resistivity, conductivity, gamma ray, and delta T plotted alongside a temperature log and lithologic log by depth for the USU Camas-1 well. SP is reported in mV, gamma ray is reported in API-GR, resistivity is reported in ohm-m, conductivity is reported in mmho/m, and delta T is reported in µsec/ft. A gap in the data between the second and third suites can be observed between the depths of 492.3 and 504.4 m

at ~ 357.5 m (Fig. 5), indicating a permeable zone that received the cold injected water at this depth.

Chemical properties

Major ion analysis of the USU Camas-1 sample shows the water is dominated by sodium and bicarbonate (Table 1). Thermal water in the area has alkaline pH and higher concentration of fluorine ions, making this water chemically similar to the thermal waters that

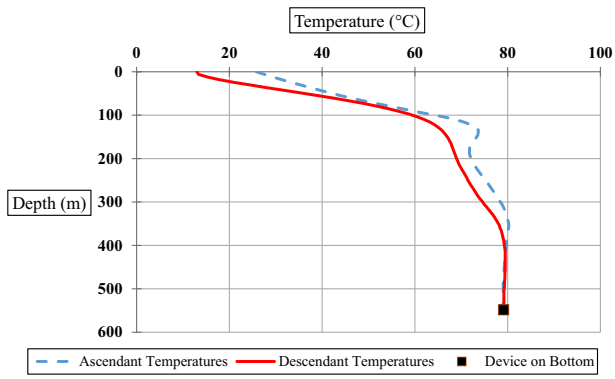

Fig. 4 Plot of temperature survey conducted on October 24, 2019. The solid red line represents temperatures recorded during the HOBO device's descent down the borehole, while the dotted blue line represents temperatures recorded during its ascent. The black square represents the 10-min period during which the HOBO device was left on the bottom of the hole

interacted with the Idaho batholith in areas north of the Prairie (Mariner et al. 2006). Moreover, the Idaho batholith is the basement rock underlying the sediments and volcanics in the Camas Prairie area (Cluer and Cluer 1986; Garwood et al. 2014).

Trilinear (Piper 1944) diagrams (Fig. 7a, b) show that the USU Camas-1 sample, which is the only new data point, plots in the same region as all but two of the other Camas Prairie samples (Mattson et al. 2016) and the Kimberly, but not Kimama or Mountain Home, samples of Project Hotspot (Freeman 2013). The USU Camas-1 $\delta^{18}O$ and $\delta^{2}H$ values plot with other local samples and Kimama on a local meteoric water line (LMWL) represented by the equation $\delta^{2}H = 7.125*\delta^{18}O\text{-}15.5$ (Fig. 8) lying below the GMWL (Craig 1961), indicating that the water has a meteoric component.

Reservoir temperature

Reservoir temperature estimates based on the Na–K and K–Mg cation geothermometers can be compared on a ternary "Giggenbach diagram" to assess the reliability of these estimates due to the degree of water–rock equilibrium and mixing with cooler groundwaters (Giggenbach 1988). The USU Camas-1 groundwater composition plots near the Mg apex, similar to the Kimama and Kimberly samples (Fig. 9), indicating that the reservoir temperature estimates using these thermometers are unreliable. These waters have either experienced significant mixing with Mg-rich cool groundwater or have had incomplete re-equilibration with host rock minerals during ascent and cooling. These contrast to the Mountain Home thermal water that falls in the "partially equilibrated" field, suggesting that the estimates may be more representative, although mixing and cooling have still impacted the Mg content. Additional cation geothermometers and multicomponent geothermometry are presented below to evaluate the Camas-1 geothermal temperature potential.

Geothermometer reservoir temperature calculations range from 82 to 144 °C (Table 2). Certain geothermometers were developed for different water facies and system compositions. Thus, there is bound to be a large spread of reservoir temperatures produced when using a suite of geothermometers. For example, the Na–K–Ca–Mg (Fournier and Potter 1979) geothermometer makes corrections to the Na–K–Ca geothermometer (Fournier

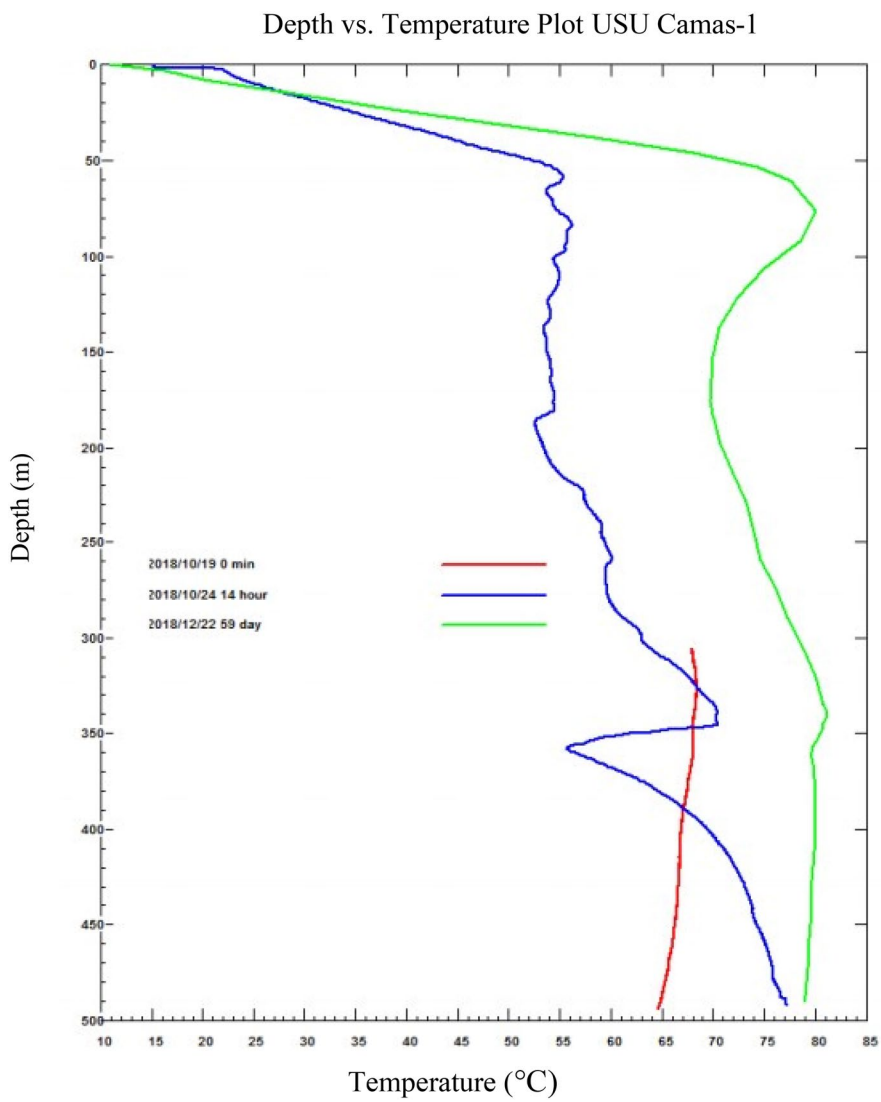

Fig. 5 Temperature versus depth plots. Conducted under shut-in conditions following the injection of cold water into the USU Camas-1 well. The red line represents the brief and partial temperature data recorded at the start of the injection. The blue line represents the temperature run that occurred at 14 h following injection, and the green line delineates the temperature run that commenced 59 days after injection (adapted from Garg and Goranson 2018)

and Truesdell 1973) to account for the presence of magnesium. The Na–K–Ca geothermometer (Fournier and Truesdell 1973) appears to be reliable for the USU Camas-1 system, because that geothermometer is more accurate for water that equilibrated at temperatures exceeding 100 °C, and for systems with abundant calcium-bearing minerals. The USU Camas-1 core contained much secondary calcite mineralization (Smith 2022). Based on the Na–K–Ca geothermometer result (Table 2), the USU Camas-1 water equilibrated at a reservoir temperature of 125 °C. The quartz (Fournier 1977) and the Na–K (Fournier 1979) geothermometers produce similar reservoir temperatures of 126 °C and 123 °C, respectively.

Multicomponent geothermometric (RTEst) temperature estimate for this geothermal system is given in Fig. 10 where solubility curves of various minerals converge

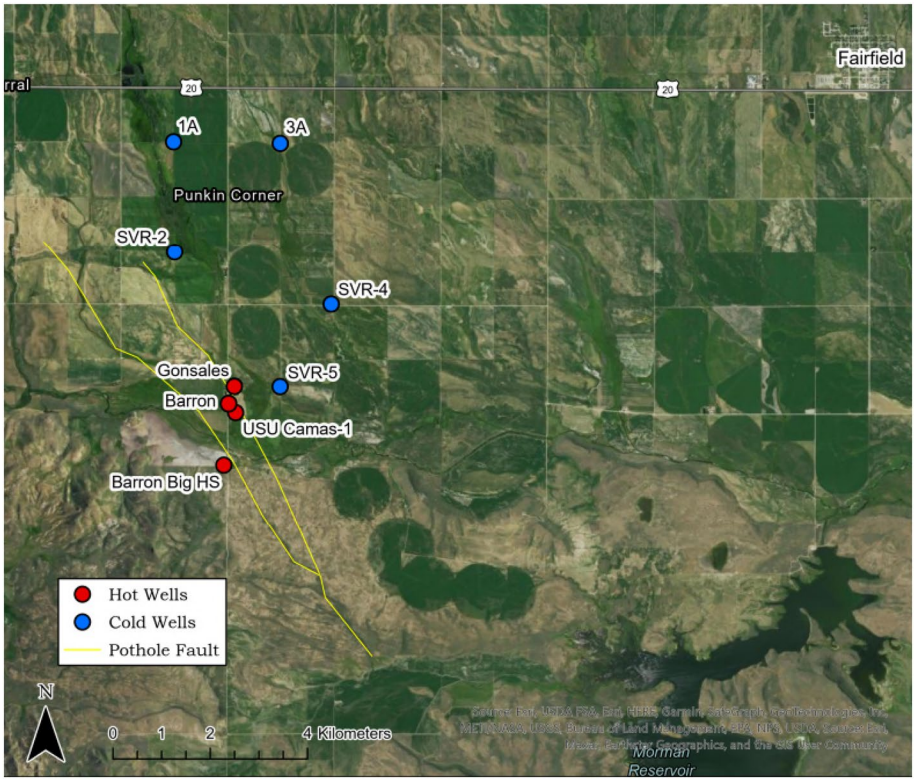

Fig. 6 Map of Camas Prairie depicting hot and cold well locations. The orientation of the Pothole fault per Shervais et al. (2017) also is shown

Table 1 Chemical analyses of USU Camas-1 and Project Hotspot (Freeman 2013) water samples

Sample	T (°C)	EC (µS/cm)	pH (units)	Alkalinity (mg/L as $CaCO_3$)	Ca	Mg	Na	K	Cl	SO_4	SiO_2
USU Camas-1	71.9	925	8.76	164	2.29	0.17	97.5	2.53	11.7	13.5	81.2
KA-1	28.8	1060	8.17	120	21.1	3.21	284	10.3	315	306	158
KB-38	23.3	2970	7.60	1100	24.7	10.1	562	17.9	204	7.29	94.5
KB-52	15.6	1765	7.72	950	15.4	5.43	363	9.38	128	14.1	71.6
KB-63	17.7	2568	7.83	850	23.8	9.33	541	13.2	189	13.8	76.7
MH-5,726	31.3	870	9.59	100	8.71	0.16	288	9.02	74.8	477	196

All units in mg/L unless otherwise noted

at ~ 115 °C. Previously, Neupane et al. (2017) reported temperature estimates ranging from 103 to 108 °C for the Barron Hot Springs geothermal system in the area. Also, the RTEst temperature estimate agrees most closely with the three traditional geothermometers that produced consistent temperatures around ~ 125 °C (Table 2).

Discussion

Driller reports describe a productive zone at ~ 346.9 m. Resistivity, conductivity and SP responses near 346.9 m also suggest that the rocks are permeable at this depth (Fig. 3). Resistivity drops to nearly zero ohm-m, while conductivity and SP spike. Delta T also peaks at ~ 346.9 m. The maximum temperature recorded in the USU Camas-1

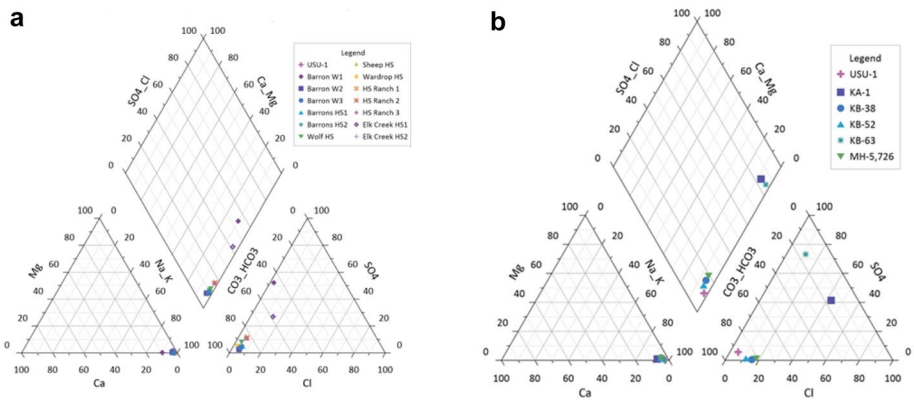

Fig. 7 Piper (1944) diagrams for the USU Camas-1 water sample. Comparison with: **a** other Camas Prairie water samples (Mattson et al. 2016), and **b** Project Hotspot water samples (Freeman 2013)

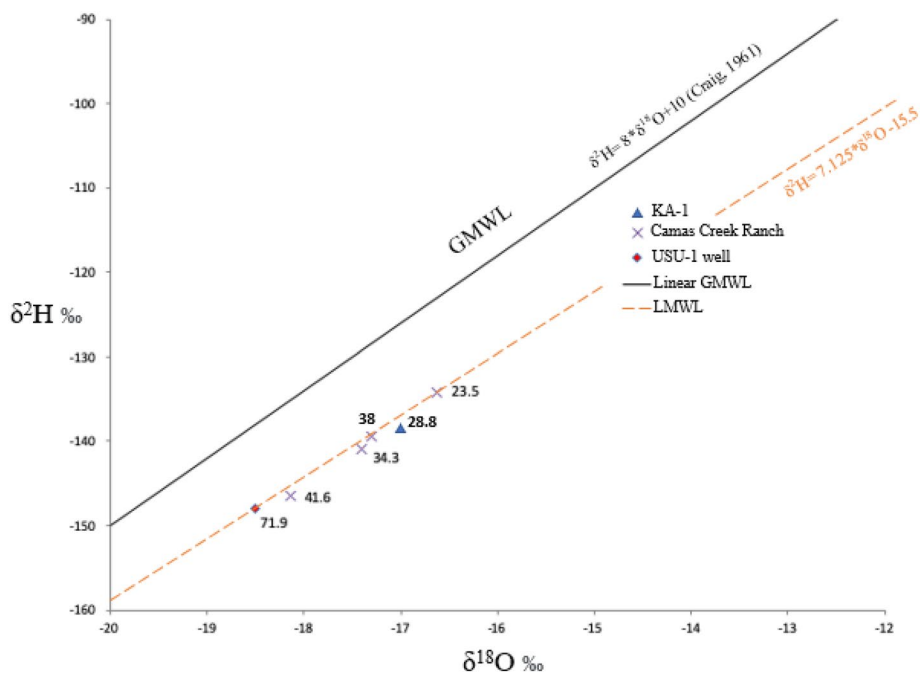

Fig. 8 Stable isotope plot of Camas Prairie water samples with the GMWL (Craig 1961). All samples are marked with measured temperatures in °C

well was 80.3 °C at ~ 353.6 m (Fig. 4). The isothermal gradient below ~ 353.6 m suggests that geothermal fluids are not flowing into the USU Camas-1 well below this depth, and that no faults supplying geothermal fluids were intersected below the productive zone. A temperature log run 14 h after injecting cold water into the well (Fig. 5) shows a temperature depression at ~ 357.5 m, likely indicating that the permeable zone accepted the cold injected fluid. The next temperature log was run 59 days after injection. The sharp decrease in temperature centered at ~ 357.5 m in the 14-h log has more or less disappeared. Presumably, the well had warmed up. Based on all of these data, it appears that a productive zone exists at ~ 357.5 m. The zone may extend from ~ 346.9 to ~ 357.5 m.

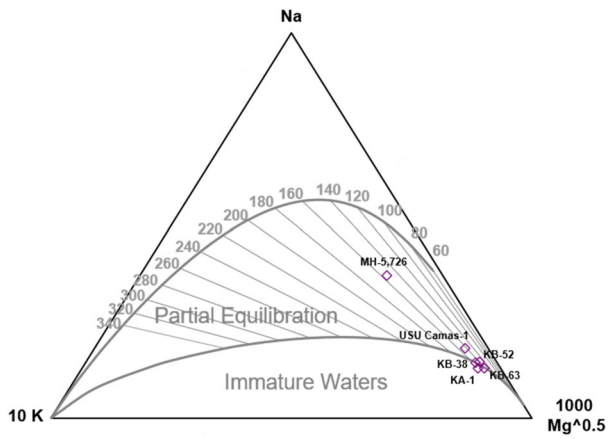

Fig. 9 Giggenbach (1988) plot of the USU Camas-1 water sample, compared to the Mountain Home, Kimama, and Kimberly samples (Freeman 2013). USU Camas-1 plots close to the Mg apex and far from the region indicating full water-reservoir mineral equilibration, indicating unreliable temperature estimates using these geothermometers

Table 2 Geothermometer calculations for USU Camas-1 and Project Hotspot (Freeman 2013) wells

Well	Quartz[1]	Chalcedony[1]	Na/K[2]	Na/K[3]	Na–K–Ca[4]	Na–K–Ca–Mg[5]	K^2/Mg^3
USU Camas-1	126	98	123	144	125	97	82
KB-38	134	107	135	155	142	86	80
KB-52	119	91	123	143	130	90	72
KB-63	123	95	120	140	130	83	73
MH-5,726	179	157	134	154	139	133	117
KA-1	164	141	143	163	139	125	80

All values in °C

[1] Fournier, 1977

[2] Fournier, 1979

[3] Giggenbach, 1988

[4] Fournier and Truesdell, 1973

[5] Fournier and Potter, 1979

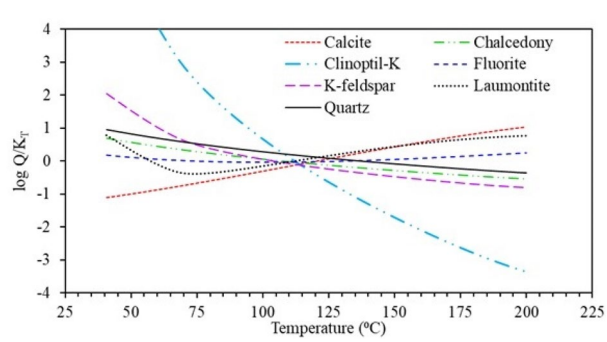

Fig. 10 Multicomponent geothermometric temperature estimate (~ 115 °C). Mineral assemblage consists of calcite, chalcedony, K-clinoptilolite, K-feldspar, fluorite, laumontite, and illite (used to swap for Mg and not shown in the diagram)

The transmissivity of USU Camas-1 estimated by Garg and Goranson (2018) is ~ 0.25–1 cm^2/s. This modest transmissivity likely means the permeability of the zone at ~ 357.5 m is relatively high. A seasonal artesian flow rate of ~ 0.7 L/s was measured (Smith 2022), supporting the presence of a permeable zone intersected by the well, likely at ~ 357.5 m.

Groundwater wells in the area around USU Camas-1 vary in temperature with location (Fig. 6). The hotter wells are located south of the colder wells, and to the west of and closer to the Pothole fault as depicted by Shervais et al. (2017). The Gonsales and SVR-5 wells are the two hot and cold wells located nearest to each other (Fig. 6). The source supplying the hot wells terminates at a point between these two wells, which are ~ 0.7 km apart.

Geothermal fluids potentially appear to be flowing upward along the Pothole fault and/or the range-front fault (Mitchell 1976), with the former preventing flow across it to the northeast. Recent $^{40}Ar/^{39}Ar$ dating of basalt from The Pothole produced an age of 692 ka (Shervais et al. 2018), demonstrating that both the Pothole fault and the range-front fault were active during the late Pleistocene. The young basalts and elevated $^{3}He/^{4}He$ ratios of ~ 2 R/R_a (Dobson et al. 2015) indicate that the heat source of Camas Prairie probably is magmatic. However, the Pothole fault and/or the range-front fault may be acting as a conduit for geothermal fluids to rise from great depth without a shallow magmatic source being present.

Three recent geothermal exploration wells were drilled in the SRP for Project Hotspot (Fig. 1). The most promising was at the Mountain Home Air Force Base (MH-2). The Mountain Home well has the highest geothermal gradient at ~ 73 °C/km, and a maximum recorded temperature of 149 °C (Lachmar et al. 2019). The Kimama well (KA-1) had a geothermal gradient of 72–75 °C/km below 960 m depth, but above that depth, the gradient was suppressed to ~ 4.5 °C/km by a massive cold water aquifer, limiting the maximum recorded temperature to 59 °C (Lachmar et al. 2017). The Kimberly (KB-1) well was the least promising, with gradients of 15 °C/km in the upper section and 5 °C/km in the lower section, and a maximum recorded temperature of 57 °C (Freeman 2013). Geothermometry results were most favorable for Mountain Home, with a calculated reservoir temperature of 133–157 °C, and Kimama, with a calculated reservoir temperature between 125 °C and 140 °C, while the lowest calculated reservoir temperature was that of Kimberly, at 113–130 °C (Freeman 2013).

Conclusions

Camas Prairie was identified using PFA as a potential geothermal resource. An exploration well, USU Camas-1, was drilled to a TD of 618.3 m near the southern end of the Pothole fault system, which PFA indicated as being the most favorable area in terms of geothermal potential. MT surveys indicated a clay seal at ~ 300 m (Glen et al. 2017). Furthermore, equilibrium reservoir temperatures of ~ 110 °C (Neupane et al. 2014, 2017) were estimated at target depths as shallow as 500–700 m.

The necessary components of a geothermal system are present at Camas Prairie. MT data suggesting the existence of a clay seal were confirmed by the presence of clayey sand, sandy clay and clay layers encountered near the bottom of the basin-fill sediment occupying the upper 314 m of the well. Heat and permeability clearly are present as well.

A productive zone was encountered in USU Camas-1 within the interval from ~ 346.9 to ~ 357.5 m. Temperatures up to 80.3 °C were measured in this zone. A moderate transmissivity of ~ 0.25–1 cm^2/s estimated from the injection test, as well as the ~ 0.7 L/s artesian flow rate, further corroborate permeability.

Camas Prairie is a promising area in terms of geothermal reservoir features, but it does not have the same potential as Mountain Home (Lachmar et al. 2019). The maximum temperature for MH-2 (~ 140 °C) is higher than USU Camas-1 (~ 80 °C). Kimberly and USU Camas-1 likely have similar reservoir temperatures based on the similarity of their hydrochemical facies from the Piper (1944) and Giggenbach (1988) diagrams (Figs. 7b and 9), and their comparable geothermometer results (Table 2). Both the conventional and multicomponent geothermometers suggest the temperature of the reservoir in which the USU Camas-1 water equilibrated is likely ~ 120 °C, which is similar to the ~ 113–130 °C reservoir temperature estimated for Kimberly (Freeman 2013).

Acknowledgements
The authors would like to thank the two anonymous reviewers and editor Luis Carlos Gutiérrez-Negrín, whose insights and suggestions greatly improved the final version of this work.

Author contributions
GN, PFD, and DLN collected the water samples, DLN performed the stable isotopic analyses, and CJS and TEL interpreted the analytical results. SKG interpreted the results of the injection test. JWS, DLN, and JPE served as the principal investigators, and logged core on- and off-site along with CJS, and also performed the XRD analyses. LLM obtained some of the temperature logs. All authors read and approved the final manuscript.

Funding
This work is part of the Snake Play Fairway project funded by the US Department of Energy under Award EERE-0006733, and Utah State University.

Availability of data and materials
The datasets supporting the conclusions of this article are available in the Utah State University Libraries Digital Commons repository at http://digitalcommons.usu.edu/.

Declarations

Competing interests
The authors declare that they have no competing interests.

Received: 30 March 2023 Accepted: 15 July 2023
Published online: 04 August 2023

References

Bethke CM, Yeakel S. The Geochemist's workbench user's guide, release 9.0. Champaign: Aqueous Solutions LLC; 2013.
Blackwell DD. Regional implications of heat flow of the Snake River Plain, northwestern United States. Tectonophysics. 1989;164:323–43.
Blackwell DD, Richards M. Geothermal map of North America. American Association of Petroleum Geologists. 2004. (scale 1:6,500,000).
Clemens DM, Wood SH. Late Cenozoic volcanic stratigraphy and geochronology of the Mount Bennett Hills, central Snake River Plain. Idaho Isochron West. 1993;60:3–14.
Cluer JK, Cluer BL. The late Cenozoic Camas Prairie rift, south-central Idaho. Geology. 1986;24:91–101.
Craig H. Isotopic variations in meteoric waters. Science. 1961;133:1702–3.
DeAngelo J, Shervais JW, Glen JM, Dobson PF, Liberty LM, Siler D, Neupane G, Newell DL, Gasperikova E, Peacock JR, Sonnenthal E, Nielson DL, Garg SK, Schermerhorn WD, Earney TE. Snake river Plain Play Fairway Analysis phase 1 favorability model (DE EE0006733). USGS Data Release. 2021a. https://doi.org/10.5066/P95EULTI.
DeAngelo J, Shervais JW, Glen JM, Dobson PF, Liberty LM, Siler D, Neupane G, Newell DL, Gasperikova E, Peacock JR, Sonnenthal E, Nielson DL, Garg SK, Schermerhorn WD, Earney TE. Snake river plain play fairway analysis phase 2 favorability model (DE EE0006733). USGS Data Release. 2021b. https://doi.org/10.5066/P9Y8MEZY.
Dobson PF, Kennedy BM, Conrad ME, McLing TL, Mattson ED, Wood TR, Cannon CJ, Spackman R, van Soest M, Robertson M. He isotopic evidence for undiscovered geothermal systems in the Snake River Plain. 40th workshop on geothermal reservoir engineering. Stanford: Proceedings; 2015:798–804.
Doherty J. PEST, model-independent parameter estimation, user manual. 5th ed. Brisbane: Watermark Numerical Computing; 2005.
Doherty J. Addendum to the PEST manual. Brisbane: Watermark Numerical Computing; 2013.

Fournier RO. Chemical geothermometers and mixing models for geothermal systems. Geothermics. 1977;5:41–50.
Fournier RO. A revised equation for Na-K geothermometer. Geotherm Res Counc Trans. 1979;3:221–4.
Fournier RO, Truesdell A. An empirical Na-K-Ca geothermometer for natural waters. Geochim Cosmochim Acta. 1973;37:1255–75.
Fournier RO, Potter RW. Magnesium correction to the Na-K-Ca chemical geothermometer. Geochim Cosmochim Acta. 1979;43:1543–50.
Freeman TG. Evaluation of the geothermal potential of the Snake River Plain, Idaho, based on three exploration holes. MS Thesis. Logan: Utah State University; 2013.
Garg SK, Goranson C. Analysis of downhole data from USU Camas-1 well. Utah State University; 2018.
Garwood DL, Kauffman JD, Othberg KL, Lewis RS. Geologic map of the Fairfield 30 x 60 minute quadrangle. Idaho Geological Survey. 2014. (scale 1:100,000).
Gaschnig RM, Vervoort JD, Lewis RS, Tikoff B. Isotopic evolution of the Idaho batholith and Challis intrusive province, northern US Cordillera. J Petrol. 2011;52:2397–429.
Gehre M, Geilmann H, Richter J, Werner R, Brand W. Continuous flow 2H/1H and 18O/16O analysis of water samples with dual inlet precision. Rapid Commun Mass Spectrom. 2004;18:2650–60.
Giggenbach WF. Geothermal solute equilibria: derivation of Na-K-Mg-Ca geoindicators. Geochim Cosmochim Acta. 1988;52:2749–65.
Glen JM, Liberty LM, Gasperikova E, Siler D, Shervais JW, Ritzinger B, Athens N, Earney TE. Geophysical investigations and structural framework of geothermal systems in west and southcentral Idaho; Camas Prairie to Mountain Home. 42nd workshop on geothermal reservoir engineering. Stanford: Proceedings; 2017:1021–33.
Honjo N. Geology and stratigraphy of the Mount Bennett Hills, and the origin of west-central Snake River Plain rhyolites. PhD dissertation. Houston: Rice University; 1990.
Kiilsgaard TH, Lewis RS. Plutonic rocks of Cretaceous age and faults in the Atlanta lobe of the Idaho batholith, Challis Quadrangle. Symposium on the geology and mineral deposits of the Challis 1°x2° Quadrangle, Idaho. Spokane: Proceedings; Washington Geological Survey Bulletin 1658. 1985:29–42.
Lachmar TE, Freeman TG, Sant CJ, Walker JR, Batir JF, Shervais JW, Evans JP, Nielson DL, Blackwell DD. Effect of an 860-m thick, cold, freshwater aquifer on geothermal potential along the axis of the eastern Snake River Plain. Idaho Geothermal Energy. 2017;5:28.
Lachmar TE, Freeman TG, Kessler JA, Batir JF, Evans JP, Nielson DL, Shervais JW, Chen X, Schmidt DR, Blackwell DD. Evaluation of the geothermal potential of the western Snake River Plain based on a deep corehole on the Mountain Home AFB near Mountain Home. Idaho Geothermal Energy. 2019;7:26.
Mariner RH, Evans WC, Young HW. Comparison of circulation times of thermal waters discharging from the Idaho batholith based on geothermometer temperatures, helium concentrations and 14C measurements. Geothermics. 2006;35:3–25.
Mattson ED, Conrad ME, Neupane G, McLing TL, Wood TR, Cannon CJ. Geothermometry mapping of deep hydrothermal reservoirs in southeastern Idaho: Final report, Appendices B & C. Idaho National Laboratory; 2016.
Mitchell JC. Geothermal investigations in Idaho, part 7, geochemistry and geologic setting of the thermal waters of the Camas Prairie area, Blaine and Camas Counties Idaho. Idaho Department of Water Resources, Water Information Bulletin No. 30; 1976: 44 p.
Neupane G, Mattson ED, McLing TL, Palmer CD, Smith RW, Wood TR. Deep geothermal reservoir temperatures in the eastern Snake River Plain, Idaho using multicomponent geothermometry. 39th workshop on geothermal reservoir engineering. Stanford: Proceedings; 2014:831–42.
Neupane G, Baum JS, Mattson ED, Mines GL, Palmer CD, Smith RW. Validation of multicomponent equilibrium geothermometry at four geothermal power plants. 40th workshop on geothermal reservoir engineering. Stanford: Proceedings; 2015:842–58.
Neupane G, Mattson ED, Spycher N, Dobson PF, Conrad ME, Newell DL, McLing TL, Wood TR, Cannon CJ, Atkinson TA, Brazell CW, Worthing WC. Geochemical evaluation of geothermal resources of Camas Prairie, Idaho. 42nd workshop on geothermal reservoir engineering. Stanford: Proceedings; 2017:897–908.
Nielson DL, Shervais JW. Conceptual model for Snake River Plain geothermal systems. 39th workshop on geothermal reservoir engineering. Stanford: Proceedings; 2014:1086–92.
Palmer CD, Ohly SR, Smith RW, Neupane G, McLing TL, Mattson ED. Mineral selection for multicomponent geothermometry. Geotherm Res Counc Trans. 2014;38:453–9.
Piper AM. A graphic procedure in the geochemical interpretation of water-analyses. American Geophys Union Trans. 1944;25:914–28.
Shell Exploration and Production. Play based exploration guide. Rijswijk: Graphics Media and Publishing Services (GMP); 2013.
Shervais JW, Shroff G, Vetter SK, Matthews S, Hanan BB, McGee JJ. Origin and evolution of the western Snake River Plain: Implications from stratigraphy, faulting, and the geochemistry of basalts near Mountain Home, Idaho. Tectonic and magmatic evolution of the Snake River Plain volcanic province. Bonnichsen B, White CM, McCurry M. eds. Idaho Geological Survey Bulletin 30. 2002:343–61.
Shervais JW, Glen JM, Dobson PF, Gasperikova E, Sonnenthal E, Visser C, Nielson DL, Garg SK, Evans JP, Siler D, DeAngelo J, Athens N, Burns E. Snake river plain play fairway analysis—phase 1 report. Geotherm Res Counc Trans. 2015;39:761–7.
Shervais JW, Glen JM, Nielson DL, Garg SK, Dobson PF, Gasperikova E, Sonnenthal E, Visser C, Liberty LM, DeAngelo J, Siler D, Evans JP. Geothermal Play Fairway Analysis of the Snake River Plain: Phase 1. 41st workshop on geothermal reservoir engineering. Stanford: Proceedings; 2016:1997–2003.
Shervais JW, Glen JM, Nielson DL, Garg SK, Liberty LM, Siler D, Dobson PF, Gaperikova E, Sonnenthal E, Neupane G, DeAngelo J, Newell DL, Evans JP, Snyder N. Geothermal Play Fairway Analysis of the Snake River Plain: Phase 2. Geotherm Res Counc Trans. 2017;41:2328–45.
Shervais JW, Glen JM, Siler D, DeAngelo J, Liberty LM, Nielson DL, Garg SK, Neupane G, Dobson PF, Gasperikova E, Sonnenthal E, Newell DL, Evans JP, Snyder N, Mink LL. Provisional conceptual model of the Camas Prairie (ID)

geothermal system from Play Fairway Analysis. 43rd workshop on geothermal reservoir engineering. Stanford: Proceedings; 2018:1600–7.
Shervais JW, Glen JM, Siler D, Liberty LM, Nielson DL, Garg SK, Dobson PF, Gasperikova E, Sonnenthal E, Newell DL, Evans JP, DeAngelo, J, Peacock JR, Earney TE, Schermerhorn WD, Neupane G. Play Fairway Analysis in geothermal exploration: The Snake River Plain volcanic province. 45th workshop on geothermal reservoir engineering. Stanford: Proceedings; 2020:186–94.
Smith CJ. Evaluation of the geothermal potential of the Camas Prairie, south-central Idaho. MS Thesis. Logan: Utah State University; 2022.
Smith RB, Braile LW. The Yellowstone hotspot. J Volcanol Geoth Res. 1994;61:121–87.
Smith RB, Jordan M, Steinberger B, Puskas CM, Farrell J, Waite GP, Husen S, Chang W, O'Connell R. Geodynamics of the Yellowstone hotspot and mantle plume: seismic and GPS imaging, kinematics, and mantle flow. J Volcanol Geoth Res. 2009;188:26–56.
US Geological Survey. National field manual for the collection of water-quality data. US Geological Survey Techniques of Water-Resource Investigations 09-A4; 2006, p. 166.
Western Governors' Association. Geothermal Task Force Report; 2006, p. 66.

Publisher's Note